High-Intensity Laser–Plasma Interactions in the Refluxing Limit

Introduction

Studies of energy transfer from high-intensity laser pulses into solid-density targets address basic issues in laser–plasma interactions, including electron acceleration, ion acceleration, and secondary radiation generation.[1–5] At laser irradiances $I\lambda^2 > 10^{18}$ (W/cm^2)μm^2, where I is the laser intensity and λ is the laser wavelength, electrons are accelerated to relativistic energies and can be used to create unique states of matter. These studies are motivated by a variety of applications in high-energy-density science,[6] including bright backlighter source development[7] and advanced inertial confinement fusion schemes such as fast ignition.[8,9]

Many uncertainties exist in the transport and energy deposition of laser-generated high-current electron beams in dense plasmas. Their propagation is strongly affected by self-generated electromagnetic fields and the ability of the plasma to draw a return current.[10–17] Simple, well-characterized target geometries can identify the dominant laser–plasma and energy-deposition phenomena and can be used for detailed code benchmarking. Of particular interest are methods for isochorically heating solid-density targets to hundreds of eV and many keV using fast electrons[18–24] to infer laser–plasma coupling and heating as a function of laser intensity, wavelength, pulse duration, and preplasma scale length.[25–33]

The fast electrons generated during high-intensity laser–plasma interactions with solid targets of just tens or hundreds of microns in extent and less than a few microns in thickness rapidly create a solid-density, high-energy-density plasma.[25,26] The electrons typically have energies of up to a few MeV and ranges of many hundreds of microns—far greater than the target thickness. The Debye sheath fields that rapidly form at the target surfaces constrain the majority of fast electrons to multiple transits through the target. This process is known as refluxing[3,34,35] and is a particularly efficient mechanism for transferring fast-electron energy into thermal-plasma energy prior to any significant hydrodynamic disassembly.[27–29]

Refluxing in small-mass targets provides a simple geometry for testing laser coupling, fast-electron generation, and plasma-heating models. For example, K-shell spectroscopy using buried fluors, a widely used technique for diagnosing fast-electron transport in massive solid targets,[18,21–23,33,36–38] is not necessary here. The target is so small that by choosing an appropriate mid-Z material (to simplify the ion de-excitation cascades and reabsorption of fluorescent x rays[21,37,39]), the target is the fluor. This is a unique property of the refluxing limit and provides insightful simplifications to the modeling of fast-electron stopping and secondary radiation generation and transport.[28]

Theobald *et al.*[27] have shown that the energy in K$_\alpha$ emission, per joule of laser energy, from a small-mass target is insensitive to the fast-electron spectrum and laser intensity in the relativistic regime. Myatt *et al.*[28] have published modeling of these experiments, taking into account the effect of spatial and temporal gradients, target expansion and heating, and fast-electron refluxing on the absolute and relative emission of K$_\alpha$ and K$_\beta$ fluorescent lines. This is used to infer the laser-to-electron energy-conversion efficiency $\eta_{L\to e}$, accounting for classical fast-electron stopping and relativistic K-shell ionization cross sections.[40]

This article describes experiments that demonstrate the effect of bulk heating on L $\longrightarrow$ K and M $\longrightarrow$ K electron transitions in small-mass copper targets. It has previously been demonstrated using high-resolution K$_\alpha$ spectroscopy that high bulk-electron temperatures can be achieved (hundreds of eV) in a refluxing geometry.[25,26] In our experiment, variations in the K$_\beta$/K$_\alpha$ ratio as a function of target volume diagnose the bulk-electron temperature during the rapid isochoric heating phase. This allows the laser-to-electron energy-conversion efficiency $\eta_{L\to e}$ to be inferred by comparing experimental K$_\beta$/K$_\alpha$ measurements to numerical target-heating calculations, in addition to inferring the conversion efficiency from the absolute K$_\alpha$ yield.

This is a robust technique for inferring the deposited fraction of laser energy into the target bulk by fast electrons, which is required to create the experimentally observed K-photon yields. In the cold material limit, a laser-to-electron energy-conversion efficiency of $\eta_{L \to e} = (20 \pm 10)\%$ has been inferred. Laser pulses of 5 J and 1 ps at intensities of $I > 10^{19}$ W/cm^2 are shown to heat smaller-volume targets, culminating in $20 \times 20 \times 2$-μm^3 copper targets reaching the highest bulk-electron temperatures of $T_e > 200$ eV. An average laser-to-electron energy-conversion efficiency of around 20% has been inferred over a wide range of target volumes, in good agreement with cold K$_\alpha$ measurements.

The following sections (1) describe the experimental setup; (2) compare K$_\alpha$-emission measurements to a model of K$_\alpha$ production from small-mass targets; (3) compare bulk-heating measurements with numerical target-heating calculations; and (4) provide a discussion and summary.

Experimental Setup

The experiments were performed using the Multi-Terawatt (MTW) Laser System at the Laboratory for Laser Energetics. MTW is a hybrid laser system, which operates in the conventional chirped-pulse–amplification (CPA) mode and combines optical parametric amplification (OPA) with Nd-doped laser-glass amplification.[41] The measured contrast ratio after the OPCPA stage is around 10^8 during the 100-ps period prior to the main laser pulse. Maximum output energies >10 J in a transform-limited subpicosecond pulse duration provide peak powers of the order of 10 TW. The energy in the laser pulse, the pulse duration, and the spatial distribution of the laser beam on the compressor output are monitored on a shot-to-shot basis. Typical short-term stability over a period of a few days is 3% rms in energy and 10% rms in the pulse duration.

For the experiments described here, the laser delivered 1- to 5-J, 1-ps pulses and was focused at normal incidence onto planar-foil targets using an $f/2$ off-axis parabola. The focal-spot full width at half maximum was between 4 to 6 μm and provided a peak intensity of up to 2×10^{19} W/cm^2. The targets were copper foils that ranged in cross-sectional area and thickness between $20 \times 20 \times 2$ μm^3 and $500 \times 500 \times 50$ μm^3. Two types of target mounts were used, depending on the target size: 1- to 2-μm-diam spider-silk threads and 17-μm-diam silicon carbide stalks.

Measurements of the time-integrated copper K$_\alpha$ (8.05-keV) and copper K$_\beta$ (8.91-keV) emission were performed using a spectrometer based on an x-ray charge-coupled-device (CCD)

camera operating in the single-photon–counting mode.[42] The spectrometer was located 23° to the target front-surface normal and incorporated extensive lead shielding and collimation tubes to optimize the signal to noise and minimize the detection of hard x-ray photons. It is assumed that K photons are emitted uniformly over 4π steradians and only weakly attenuated by the target plasma itself, prior to reaching the spectrometer. Copper filters of 75- to 150-μm thickness attenuated the K-shell emission, allowing K$_\alpha$ and K$_\beta$ photons to be transmitted just below the K edge of the filter. The final K-shell spectrum is calculated taking into account the solid angle sampled by the detector, the x-ray CCD quantum efficiency, and the filter transmission.

Measurements of the K$_\alpha$ Yield

High-intensity laser pulses interact with solid-density targets in a short-density-scale-length preplasma. The collisionless absorption of laser energy into relativistic electrons occurs up to the relativistic critical-density surface through **v** $\times$ **B** acceleration, resonance absorption, vacuum heating, and parametric instabilities.[24,43–45] Electron transport and heating away from the focal spot require that the fast-electron current be opposed by an inductively or electrostatically generated electric field that draws a return current from the thermal background. At the target boundaries, escaping fast electrons rapidly form a Debye sheath that, for sufficiently small targets, provides a potential that prevents a significant fraction of fast electrons from escaping. A MeV electron, for example, which has a range of around 1 mm and a characteristic slowing-down time of approximately 1 ps at solid density, will make multiple transits across a micron-scale-thickness, solid-density plasma before stopping. The high-energy electrons essentially provide their own return current. This reduces the enhanced stopping due to resistive electric fields associated with cold return currents that are found in more-massive targets.[46,47] In this case, resistive inhibition is not important because the characteristic electron range in the resistive electric fields is greater than the foil thickness. A resistive electric field $E_{res} \approx 2 \times 10^5$ kV/cm, which is representative of interaction conditions for copper at a few hundred eV, would stop a 1-MeV electron in 50 μm, assuming a minimum conductivity $\sigma = 1 \times 10^6$ (Ωm)$^{-1}$ (Ref. 28). This resistive range is greater than the target thickness, allowing the electrons to contribute to the return current over time scales greater than their characteristic target transit time.

K$_\alpha$ emission has been used in many experiments to diagnose fast-electron-energy spectra and electron angular distributions during high-intensity laser–plasma interactions.[18,21,22,33,37] K-photon emission is generated during inelastic collisions

between fast electrons (with energies exceeding the K-shell binding energy) and electrons in the K shell. The fast-electron–induced K-shell vacancy is short lived ($<10^{-12}$ s) and decays through radiative and nonradiative de-excitation. The most important processes for mid-Z elements such as copper is the competition between Auger decay and K-shell fluorescence, which is quantified by the K-shell fluorescence probability.[48] K_α and K_β emission is thus generated during L $\longrightarrow$ K and M $\longrightarrow$ K electronic transitions.

The copper K-shell spectrum was investigated as a function of laser intensity using $500 \times 500 \times 20$-μm^3 copper targets to access the cold-material limit by using relatively large-mass targets, while keeping them thin enough to maintain the Debye sheath fields that cause refluxing and minimize opacity effects. Figure 113.1 shows a series of K_α emission measurements (normalized to the laser energy) using 1-ps-duration laser pulses over an intensity range of 5×10^{16} W/cm$^2 < I < 5 \times 10^{20}$ W/cm^2. The intensity on target is varied by changing the laser-spot size and laser energy. Data from the MTW laser (solid circles) are shown and compared to previously published data from the Vulcan PW laser (open circles).[27,28,49]
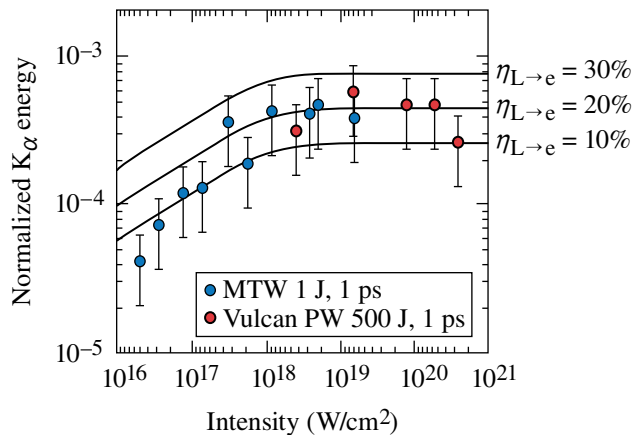
Figure 113.1
K_α energy (normalized to the laser energy) as a function of laser intensity. Data are shown for $500 \times 500 \times 20$-μm^3 copper targets from the MTW laser (solid circles) and the Vulcan PW laser (open circles).[27,28] Predictions from the K_α-production model are shown (solid lines) for laser-to-electron energy-conversion efficiencies $\eta_{L\rightarrow e}$ = 10%, 20%, and 30%.

The experimental data in Fig. 113.1 are compared to a model of K_α production (solid black lines) as described in Ref. 27. The model accounts for collisional fast-electron energy transfer only and makes no inference to the spatial homogeneity of the energy deposition, but simply allows the fast electrons to slow down. An exponential fast-electron-energy spectrum is

specified using a scaling relationship between the fast-electron temperature T_e and the laser intensity I. The ponderomotive scaling T_e [MeV] $= 0.511\left[\left(1 + I_{18}\lambda_{\mu m}^2/1.37\right)^{1/2} - 1\right]$ is used for $I > 10^{18}$ W/cm^2 (Ref. 24), where I_{18} is the laser intensity in units of 10^{18} W/cm^2 and $\lambda_{\mu m}$ is the laser wavelength in microns. Such a scaling has been shown to become increasingly less accurate at lower laser intensities and is replaced by T_e [MeV] $= 0.05\, I_{18}^{1/3}$, for interactions $I < 10^{18}$ W/cm^2. This phenomenological scaling is extrapolated from existing experimental measurements that are summarized in the review by Gibbon *et al.*[10]

The K_α-production model accounts for two distinct properties afforded by the refluxing process. The fast electrons are allowed to lose all of their energy inside the target, independent of their range, described using the classical slowing-down approximation. Energy is transferred to atomic electrons with high efficiency ($>90\%$),[28] and K-shell vacancies are created during each transit of the target by electrons with energy above the copper K-shell binding energy. This is accounted for in the K-shell ionization cross section, which is modified for relativistic effects.[39,40] There is also a correction for reabsorption of the emitted photons. The K_α transmission of a 20-μm-thick foil, for example, is 70%, which assumes a uniform fast-electron density and an attenuation length of $L = 25\ \mu$m.

The fraction of incident laser energy deposited by fast electrons in the target, which generates the observed K-photon emission, is, to a good approximation, the laser-to-electron energy-conversion efficiency $\eta_{L\rightarrow e}$, with ion acceleration effects representing a small energy correction. For laser parameters consistent with the experiments reported here, the measured conversion efficiencies of laser energy into ion acceleration (including protons from surface contamination) are in the range of 0.1% to 2% (Refs. 34, 50–52). The experimentally inferred laser-to-electron energy-conversion efficiency therefore represents, to within experimental error, a minimum of the absolute $\eta_{L\rightarrow e}$ value.

The refluxing model predicts the K_α yield as a function of laser intensity for various laser-to-electron energy-conversion efficiencies $\eta_{L\rightarrow e}$. Figure 113.1 demonstrates good agreement between the energy emitted by K_α photons (normalized to the laser energy) and the K_α-production model. A conversion efficiency of laser energy into fast electrons $\eta_{L\rightarrow e} = (20\pm10)\%$ is inferred for $I > 10^{18}$ W/cm^2. If refluxing were not considered, K-photon production would fall dramatically for $I > 10^{18}$ W/cm^2 because there is insufficient time or material in a single pass of the plasma to support appreciable fast-electron-

energy loss or significant K-shell vacancy creation with an increasing electron range.

The data show that K_α conversion efficiency is a weakly increasing function of laser intensity above $I = 10^{18}$ W/cm^2. This is also a feature of the model, caused by the interplay between the energy dependence of the K-shell ionization cross section and the insensitivity of the K_α generation mechanism to the fast-electron temperature and energy spectrum in the refluxing regime. The effect is demonstrated in both data sets using both 1-J and 500-J laser pulses with comparable 1-ps pulse durations. For $I < 10^{18}$ W/cm^2, the fast-electron temperature T_e reduces and the K_α signal is predicted to decrease with laser intensity. This is a result of the particular energy dependence of the fast-electron range and the K-shell ionization cross section. This has been confirmed experimentally by defocusing the MTW laser and entering the nonrelativistic regime.

Influence of Target Heating on K-Shell Line Emission

The bulk-electron temperature that an initially cold target reaches during refluxing is governed by the target mass and the energy content of the laser-accelerated electrons. Numerical target-heating calculations[28] predict that volumetric heating to $T_e > 100$ eV in small-mass ($<300 \times 300 \times 20$-$\mu$m^3) copper targets is sufficient to collisionally ionize and partially deplete the M shell. Filling of the K-shell vacancy from the M shell will be suppressed and provides diagnostic access to the bulk-plasma environment through variations of the K_β/K_α ratio from that expected in the cold-material limit, as shown in Fig. 113.2. This

effect can be used to provide a self-consistency check on the total fast-electron-energy content.

The variation of K_β/K_α as a function of local bulk-electron temperature is shown in Fig. 113.3, based on the calculation reported in Ref. 28, which takes into account the LTE ion population, using the code *PrismSPECT*.[53] Here, K_β/K_α is normalized to the expected cold-material value $K_\beta/K_\alpha = 0.14$. A dramatic reduction in K_β/K_α is demonstrated for bulk-electron temperatures of up to 400 eV, beyond which there are negligible numbers of ions with populated M shells and no K_β emission is possible.
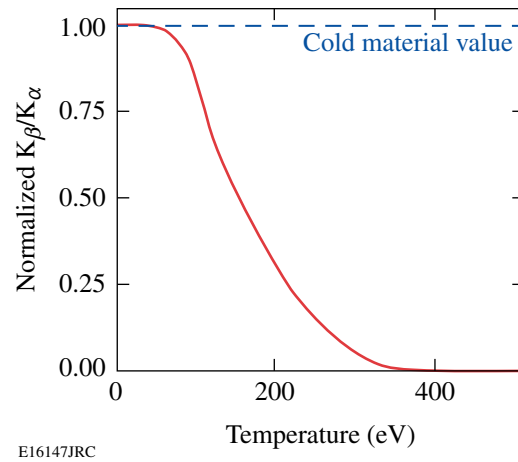

E16147JRC

Figure 113.3
K_β/K_α ratio variation with bulk-electron temperature (normalized to the cold-material value).

E16143JRC
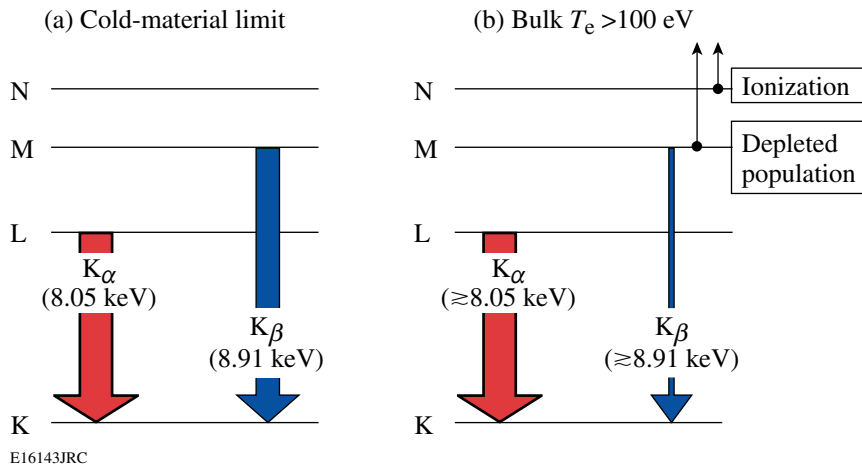
Figure 113.2
Copper-energy levels showing L $\longrightarrow$ K and M $\longrightarrow$ K electronic transitions that produce K_α and K_β radiative emission. Two examples are given: (a) a solid-density plasma in the cold-material limit (constant K_β/K_α) and (b) a solid-density plasma with bulk $T_e > 100$ eV (suppressed K_β/K_α). The number of emitted photons during L $\longrightarrow$ K and M $\longrightarrow$ K transitions is represented schematically by the relative arrow widths.

Figure 113.4 shows that the influence of bulk heating on K-shell emission predicted by the estimate in Fig. 113.3 is indeed observed experimentally. Examples of copper K-shell spectra are shown for (a) $500 \times 500 \times 50$-μm^3 and (b) $20 \times 20 \times 3$-μm^3 copper targets. The spectra were measured from interactions with 5-J, 1-ps laser pulses at an intensity of $I = 2 \times 10^{19}$ W/cm^2. The K_α and K_β peaks are fit to Gaussian line shapes with a FWHM of 220 eV. M-shell depletion in the $20 \times 20 \times 3$-μm^3 target has significantly reduced the K_β emission in comparison to that measured from the $500 \times 500 \times 50$-μm^3 target.
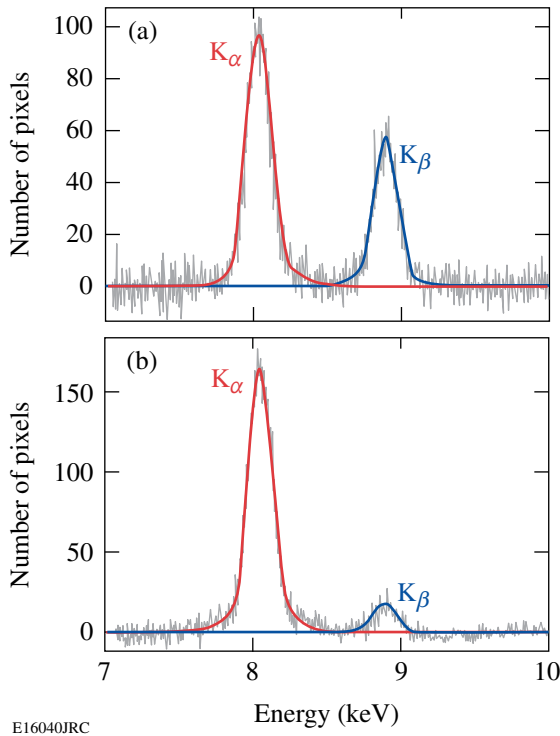

Figure 113.4
Example spectra for (a) $500 \times 500 \times 50$-μm^3 and (b) $20 \times 20 \times 3$-μm^3 copper targets and 5-J, 1-ps laser pulses at intensities $I = 2 \times 10^{19}$ W/cm^2. The K_α and K_β peaks are shown.

The copper K-shell spectrum was measured as a function of target volume for a 1-ps pulse duration and constant laser intensity of $I = 2 \times 10^{19}$ W/cm^2. This shows the variation of K_β/K_α with increasing energy density, achieved by depositing a similar amount of fast-electron energy within decreasing target plasma volumes. Figure 113.5 shows variations in the energy emitted by K_α and K_β photons (normalized to the laser energy) for target volumes of 5×10^{-6} mm$^3 < V < 1 \times 10^{-1}$ mm^3. Three distinct regions are highlighted. In region 1 ($V > 10^{-3}$ mm^3) the ratio of energy emitted in K_α and K_β is constant, consistent with the cold-material value. In region 2 (5×10^{-6} mm$^3 < V < 1 \times$

10^{-3} mm^3) the energy emitted in K_α remains approximately constant but K_β emission is increasingly suppressed for decreasing plasma volumes. This is consistent with M-shell depletion due to collisional ionization from the thermal background plasma. Any shifts in the K_β emission as M-shell electrons are being removed, however, are not resolved by our spectrometer. At sufficiently high-energy densities, achieved in region 3 ($V < 5 \times 10^{-6}$ mm^3), the energy in both K_α and K_β emission is dramatically suppressed. It is possible that for these very small targets, expansion during the period of active K-shell emission might impact the K_α and K_β yields. In all cases, a hot plasma corona of less than solid density is always present but will contribute negligibly to the total K_α and K_β signal because the emission is naturally weighted toward higher densities. Nonetheless, the total mass of the solid part is, in all cases, considerably larger than in the preplasma/corona during the time of K-shell emission. Figure 113.5 shows the insensitivity of K_α yield to target mass for volumes ranging between 5×10^{-6} to 1×10^{-3} mm^3, suggesting that a significant fraction of the target remains at solid density. Over the same range, however, K_β/K_α drops by almost an order of magnitude.
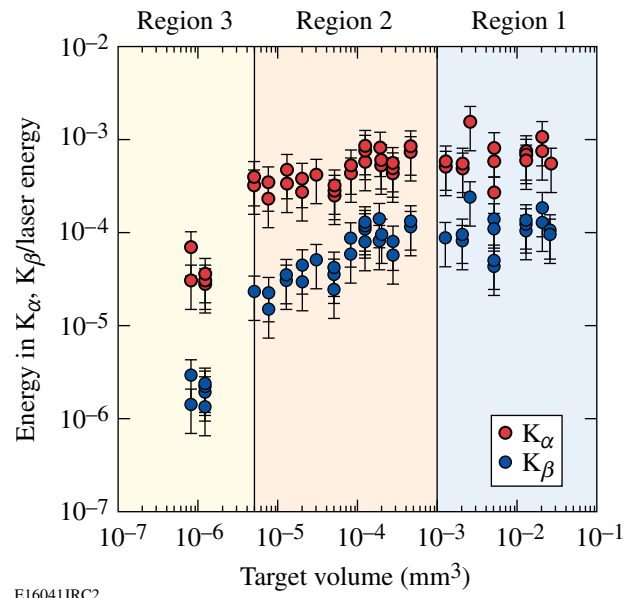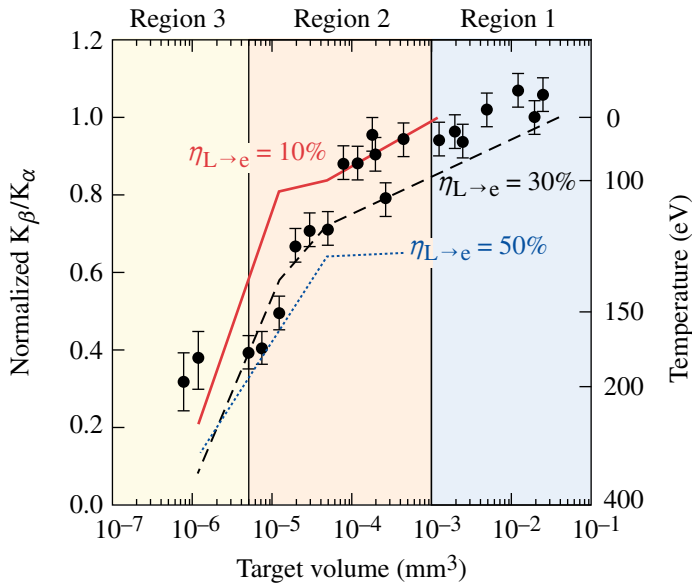

Figure 113.5
Energy in K_α and K_β (normalized to the laser energy) as a function of target volume. Three distinct regions of behavior (1, 2, and 3) in the K-photon emission are identified for increasing energy densities (see text for details).

Figure 113.6 shows the experimentally measured variation in K_β/K_α (left axis; taken from the data presented in Fig. 113.5) as a function of target volume. The error associated with each K_β/K_α value is given by the standard deviation from a number

Figure 113.6

K_β/K_α (normalized to the cold-material value—left axis) and bulk-electron temperature (right axis) as a function of target volume. Calculated K_β/K_α [assuming laser-to-electron energy-conversion efficiencies $\eta_{L \to e}$ = 10% (solid line), 30% (dashed line), and 50% (dotted line)] as a function of target volume.

of shots at a given target volume. The right axis shows the corresponding bulk-electron temperatures using the model shown in Fig. 113.3. A 3.5× reduction in K_β/K_α for target volumes $V = 10^{-6}$ mm^3 below the cold-material value is consistent with a bulk-electron temperature $T_e \approx 200$ eV. The drop in K_α yield in region 3 may indicate temperatures even greater than 200 eV, causing L-shell depletion through collisional ionization.

A thorough analysis of K_β/K_α variations requires numerical calculations to take into account the spatial and temporal variations in the fast-electron distribution and the target heating. This is achieved by combining ion-population distribution calculations from the collisional-radiative code *PrismSPECT*[53] with 3-D numerical target-heating calculations[28] using the implicit-hybrid PIC code *LSP*.[54] The fast-electron source is defined in *LSP* by promoting electrons from the cold bulk-electron population at a rate consistent with a constant fraction ($\eta_{L \to e}$) of the laser power. The use of a collisional-radiative code to calculate the ion-population distribution is justified because a copper plasma at a few hundred eV and $n_e = 10^{23}$ cm^{-3} reaches a steady state in around 1 ps and the charge-state dynamics in the plasma is governed by the thermal background, with little influence from the MeV-scale fast-electron component of the distribution function.

Results of this calculation are shown in Fig. 113.6. The calculated variation in K_β/K_α as a function of target volume is shown for $\eta_{L \to e}$ = 10% (solid line), 30% (dashed line), and 50% (dotted line). Good agreement is demonstrated between the experimental K_β/K_α measurements and numerical calculations for $\eta_{L \to e} =$

(20±10)% in the cold-material limit (region 1), consistent with the previous section (p. 4) on K_α emission. This demonstrates that the dominant physical phenomena present in the refluxing limit have been reasonably accounted for in the cold K-photon production model. On average, the variation of K_β/K_α is broadly consistent with a mean laser-to-electron energy-conversion efficiency of around 20%, except for the very smallest mass targets. For target volumes $V < 2 \times 10^{-5}$ mm^3, the theoretical curves begin to converge, making data comparisons increasingly challenging within the experimental uncertainties. Nonetheless, the significant reduction of K_β/K_α in this region below the cold-material limit remains consistent with the smallest mass targets, reaching the highest bulk-electron temperatures.

Discussion and Summary

In summary, high-temperature, solid-density plasmas have been produced and characterized on the MTW Laser System and compared to previous measurements from the Vulcan PW laser. Experiments have shown that absolute K_α yields from copper-foil targets, which are not heated significantly by the refluxing process, are constant for laser–plasma interactions in the relativistic regime. The measured K_α yields are compared to a K_α-production model, which shows good agreement, confirming the weak dependence of K_α generation on laser intensity, fast-electron temperature, and fast-electron range for $I > 10^{18}$ W/cm^2. Using this comparison, a laser-to-electron energy-conversion efficiency of $\eta_{L \to e} = (20\pm10)$% has been inferred in the cold-material limit. Variations in K_β/K_α over a range of target volumes (and energy density) for $T_e > 100$ eV have been measured. Experiments show numerical target-heating calcula-

E16434JRC2

tions are in good agreement with experimental observations over a wide range of target volumes that are broadly consistent with laser-to-electron energy-conversion efficiencies inferred from the simple K_α-production model.

The exploitation of refluxing in small-mass targets offers exciting potential. It provides a readily achievable method for the creation of extremely high-energy-density plasmas using the next generation of multikilojoule-class, high-intensity laser facilities, such as OMEGA EP.[55] These studies will provide new insights into electron generation, transport, and radiative emission of plasmas at unprecedented energy densities and under conditions relevant to fast ignition. On the basis of these experiments, the combined use of absolute K_α yields and K_β/K_α variations with increasing bulk-electron temperatures presents a method for determining the fast-electron-energy content. This implies that for picosecond-pulse-duration interactions in the relativistic regime, the laser energy is more important than the laser intensity for maximizing the fast-electron-energy content. This has far-reaching ramifications for the creation of high-energy-density plasmas using fast-electron–induced isochoric heating. Future experiments on OMEGA EP, for example, will use small-mass targets to access unprecedented energy densities using fast-electron–driven isochoric heating. Variations in the laser intensity and pulse duration up to the multikilojoule, 10-ps regime will make possible the formation of high-temperature, solid-density plasma in the 1- to 10-keV range.

ACKNOWLEDGMENT

REFERENCES

1. F. N. Beg *et al.*, Phys. Plasmas **4**, 447 (1997).

2. E. L. Clark *et al.*, Phys. Rev. Lett. **85**, 1654 (2000).

3. S. P. Hatchett, C. G. Brown, T. E. Cowan, E. A. Henry, J. S. Johnson, M. H. Key, J. A. Koch, A. B. Langdon, B. F. Lasinski, R. W. Lee, A. J. MacKinnon, D. M. Pennington, M. D. Perry, T. W. Phillips, M. Roth, T. C. Sangster, M. S. Singh, R. A. Snavely, M. A. Stoyer, S. C. Wilks, and K. Yasuike, Phys. Plasmas **7**, 2076 (2000).

4. R. D. Edwards *et al.*, Appl. Phys. Lett. **80**, 2129 (2002).

5. M. H. Key, M. D. Cable, T. E. Cowan, K. G. Estabrook, B. A. Hammel, S. P. Hatchett, E. A. Henry, D. E. Hinkel, J. D. Kilkenny, J. A. Koch, W. L. Kruer, A. B. Langdon, B. F. Lasinski, R. W. Lee, B. J. MacGowan, A. MacKinnon, J. D. Moody, M. J. Moran, A. A. Offenberger, D. M. Pennington, M. D. Perry, T. J. Phillips, T. C. Sangster, M. S. Singh, M. A. Stoyer, M. Tabak, G. L. Tietbohl, M. Tsukamoto, K. Wharton, and S. C. Wilks, Phys. Plasmas **5**, 1966 (1998).

6. B. A. Remington *et al.*, Science **284**, 1488 (1999).

7. H.-S. Park, D. M. Chambers, H.-K. Chung, R. J. Clarke, R. Eagleton, E. Giraldez, T. Goldsack, R. Heathcote, N. Izumi, M. H. Key, J. A. King, J. A. Koch, O. L. Landen, A. Nikroo, P. K. Patel, D. F. Price, B. A. Remington, H. F. Robey, R. A. Snavely, D. A. Steinman, R. B. Stephens, C. Stoeckl, M. Storm, M. Tabak, W. Theobald, R. P. J. Town, J. E. Wickersham, and B. B. Zhang, Phys. Plasmas **13**, 056309 (2006).

8. M. Tabak *et al.*, Phys. Plasmas **1**, 1626 (1994).

9. M. H. Key, Phys. Plasmas **14**, 055502 (2007).

10. P. Gibbon and E. Förster, Plasma Phys. Control. Fusion **38**, 769 (1996).

11. M. Tatarakis *et al.*, Phys. Rev. Lett. **81**, 999 (1998).

12. M. Borghesi *et al.*, Phys. Rev. Lett. **83**, 4309 (1999).

13. L. Gremillet *et al.*, Phys. Rev. Lett. **83**, 5015 (1999).

14. J. A. Koch *et al.*, Phys. Rev. E **65**, 016410 (2001).

15. Y. T. Li *et al.*, Phys. Rev. E **64**, 046407 (2001).

16. R. J. Kingham and A. R. Bell, Phys. Rev. Lett. **88**, 045004 (2002).

17. J. R. Davies *et al.*, Phys. Rev. E **56**, 7193 (1997).

18. J. D. Hares *et al.*, Phys. Rev. Lett. **42**, 1216 (1979).

19. S. J. Gitomer *et al.*, Phys. Fluids **29**, 2679 (1986).

20. B. Luther-Davies, A. Perry, and K. A. Nugent, Phys. Rev. A **35**, 4306 (1987).

21. H. Chen, B. Soom, B. Yaakobi, S. Uchida, and D. D. Meyerhofer, Phys. Rev. Lett. **70**, 3431 (1993).

22. K. B. Wharton *et al.*, Phys. Rev. Lett. **81**, 822 (1998).

23. K. Yasuike *et al.*, Rev. Sci. Instrum. **72**, 1236 (2001).

24. S. C. Wilks *et al.*, Phys. Rev. Lett. **69**, 1383 (1992).

25. G. Gregori *et al.*, Contrib. Plasma Phys. **45**, 284 (2005).

26. S. N. Chen *et al.*, Phys. Plasmas **14**, 102701 (2007).

27. W. Theobald, K. Akli, R. Clarke, J. Delettrez, R. R. Freeman, S. Glenzer, J. Green, G. Gregori, R. Heathcote, N. Izumi, J. A. King, J. A. Koch, J. Kuba, K. Lancaster, A. J. MacKinnon, M. Key, C. Mileham, J. Myatt, D. Neely, P. A. Norreys, H.-S. Park, J. Pasley, P. Patel, S. P. Regan, H. Sawada, R. Shepherd, R. Snavely, R. B. Stephens, C. Stoeckl, M. Storm, B. Zhang, and T. C. Sangster, Phys. Plasmas **13**, 043102 (2006).

28. J. Myatt, W. Theobald, J. A. Delettrez, C. Stoeckl, M. Storm, T. C. Sangster, A. V. Maximov, and R. W. Short, Phys. Plasmas **14**, 056301 (2007).

29. P. M. Nilson, W. Theobald, J. Myatt, C. Stoeckl, C. Mileham, I. A. Begishev, J. Brown, J. D. Zuegel, R. Betti, D. D. Meyerhofer, and T. C. Sangster, "Laser-to-Electron Energy Conversion Efficiency and Bulk Heating of Solid-Density Matter During High-Intensity Laser-Plasma Interactions in the Refluxing Limit," submitted to Physical Review Letters.

30. K. Eidmann *et al.*, J. Quant. Spectrosc. Radiat. Transf. **81**, 133 (2003).

31. A. Saemann *et al.*, Phys. Rev. Lett. **82**, 4843 (1999).

32. Z. Jiang *et al.*, Phys. Plasmas **2**, 1702 (1995).

33. A. Rousse *et al.*, Phys. Rev. E **50**, 2200 (1994).

34. A. J. Mackinnion, Phys. Rev. Lett. **88**, 215006 (2002).

35. R. A. Snavely, M. H. Key, S. P. Hatchett, T. E. Cowan, M. Roth, T. W. Phillips, M. A. Stoyer, E. A. Henry, T. C. Sangster, M. S. Singh, S. C. Wilks, A. MacKinnon, A. Offenberger, D. M. Pennington, K. Yasuike, A. B. Langdon, B. F. Lasinski, J. Johnson, M. D. Perry, and E. M. Campbell, Phys. Rev. Lett. **85**, 2945 (2000).

36. R. Kodama *et al.*, Phys. Plasmas **8**, 2268 (2001).

37. D. C. Eder *et al.*, Appl. Phys. B **70**, 211 (2000).

38. R. Kodama *et al.*, Nature **412**, 798 (2001).

39. M. Green and V. E. Cosslett, J. Phys. D **1**, 425 (1968).

40. H. Kolbenstvedt, J. Appl. Phys. **38**, 4785 (1967).

41. V. Bagnoud, I. A. Begishev, M. J. Guardalben, J. Puth, and J. D. Zuegel, Opt. Lett. **30**, 1843 (2005).

42. C. Stoeckl, W. Theobald, T. C. Sangster, M. H. Key, P. Patel, B. B. Zhang, R. Clarke, S. Karsch, and P. Norreys, Rev. Sci. Instrum. **75**, 3705 (2004).

43. F. Brunel, Phys. Rev. Lett. **59**, 52 (1987).

44. N. A. Ebrahim *et al.*, Phys. Rev. Lett. **45**, 1179 (1980).

45. K. Estabrook and W. L. Kruer, Phys. Fluids **26**, 1888 (1983).

46. A. R. Bell *et al.*, Plasma Phys. Control. Fusion **39**, 653 (1997).

47. F. Pisani *et al.*, Phys. Rev. E **62**, R5927 (2000).

48. W. Bambynek *et al.*, Rev. Mod. Phys. **44**, 716 (1972).

49. Previously published data[27] incorrectly accounted for photon attenuation by the target. The diagnostic observation angle with respect to the target normal was incorrectly stated as 16°; in fact it was 60° and the present data set takes the correct angle into account.

50. L. Robson *et al.*, Nat. Phys. **3**, 58 (2007).

51. J. Fuchs *et al.*, Nat. Phys. **2**, 48 (2006).

52. P. K. Patel *et al.*, Phys. Rev. Lett. **91**, 125004 (2003).

53. Prism Computational Sciences, Inc., Madison, WI 53711.

54. D. R. Welch *et al.*, Phys. Plasmas **13**, 063105 (2006).

55. C. Stoeckl, J. A. Delettrez, J. H. Kelly, T. J. Kessler, B. E. Kruschwitz, S. J. Loucks, R. L. McCrory, D. D. Meyerhofer, D. N. Maywar, S. F. B. Morse, J. Myatt, A. L. Rigatti, L. J. Waxer, J. D. Zuegel, and R. B. Stephens, Fusion Sci. Technol. **49**, 367 (2006).